

# Large-Scale, Solution-Synthesized Nanostructured Composites for Thermoelectric Applications

Biao Xu,\* Tianli Feng, Zhe Li, Wei Zheng, and Yue Wu\*

As more than one-half of worldwide consumed energy is wasted as heat every year, high-efficiency thermoelectric materials are highly demanded for the conversion of rejected heat to electricity in a reliable fashion. In the recent few decades, nanoscience has revolutionized thermoelectrics via the quantum confinement effect in electronic structures and grain-boundary scattering of heat carriers. As the gas-phase syntheses of nanomaterials are not easily scalable and solid-state syntheses are not controllable in terms of microstructures at various length scales, significant research efforts have focused on solution syntheses that can build nanostructures with well-defined size, composition, and morphology. Beyond the performance, several novel effects that benefit the portability and cost efficiency have been discovered in the solution-synthesized nanomaterials. Herein, the relevant progress is reviewed and some prospects proposed.

## 1. Introduction

The worldwide energy crisis has raised serious concerns. According to the energy flowchart reported by U. S. National Renewable Energy Laboratory (NREL), more than 60% of the consumed energy is wasted in the form of heat. Thermoelectrics can offer a viable solution to recover the rejected heat into electricity.<sup>[1]</sup> Compared to conventional thermal-energy-conversion strategies, thermoelectrics own many advantages such as no noise, no emission, no moving parts, and greater reliability. The conversion efficiency of thermoelectrics can be evaluated by the figure of merit,  $zT = S^2\sigma T/\kappa$ , in which  $S$  is the Seebeck

coefficient,  $\sigma$  is the electrical conductivity,  $T$  is the operational temperature, and  $\kappa$  is the thermal conductivity.

The first burgeoning in thermoelectrics happened when  $\text{Bi}_2\text{Te}_3$  was first discovered in the 1950s as a potential candidate working in the near-room-temperature range (300–500 K).<sup>[2]</sup> This was also the time of thriving of semiconductor science during which the established theory extensively developed and inspired the optimization of thermoelectric performance. The peak  $zT$  of  $\text{Bi}_2\text{Te}_3$  materials had increased very sluggishly from 0.5 in the 1950s to 1.0 in the 1990s. At the meantime,  $\text{PbTe}$  that possessed decent  $zT$  in the mid-temperature range (600–900 K) had been widely utilized in the radioisotope

thermoelectric generators in the spacecraft since the 1960s.<sup>[3]</sup>

The second renaissance of thermoelectrics followed the emergence of nanoscience. In the 1980s, Brus<sup>[4]</sup> discovered that the electron wave function of semiconductors is strongly localized and modified in nanosized  $\text{CdS}$  clusters, initiating the new era of nanoscience. Inspired by the quantum confinement effect, Hicks and Dresselhaus<sup>[5]</sup> theoretically proposed that finite-sized nanowire or nanosheet would have unique electronic band structures to enhance their power factor ( $S^2\sigma$ ) in the 1990s. Afterward, scientists had attempted to synthesize quantum-sized nanostructures using gas-phase techniques and construct the thermoelectric devices through micro fabrication.<sup>[6]</sup>

Later in the 2000s, the scattering of phonons, microscopic heat carriers, by the nanosized grain boundaries and the consequent reduction of thermal conductivity ( $\kappa$ ) have also been proposed and intensively investigated. At first, this concept was realized in a  $\text{AgPb}_m\text{SbTe}_{2+m}$  material containing Ag–Sb-rich nanoinclusions.<sup>[7]</sup> Soon afterward, it was demonstrated in a device of a single silicon nanowire that was synthesized via gas-phase deposition<sup>[8]</sup> and a macroscopic nanostructured  $\text{Bi}_{0.5}\text{Sb}_{1.5}\text{Te}_3$  composite using a solid-state, top-down method (planetary ball milling).<sup>[9]</sup>


As compared to conventional gas-phase methods, the solution-phase (wet-chemical) synthesis holds great advantage of low-cost and large production scale (several grams). When compared to the equally cost-efficient and scalable solid-state method, the solution method offers more delicate control over the size, composition, and morphologies of the nanoparticles. Earliest studies investigating the solution-phase synthesis of nanoparticles (wires, sheets) for thermoelectrics appeared since early 2010s. Initially, the aforementioned effects of quantum

Prof. B. Xu  
School of Chemical Engineering  
Nanjing University of Science and Technology  
Nanjing, Jiangsu 210094, China  
E-mail: xubiao@njut.edu.cn

Prof. B. Xu, Z. Li, W. Zheng, Prof. Y. Wu  
Department of Chemical and Biological Engineering  
Iowa State University  
Ames, IA 50011, USA  
E-mail: yuewu@iastate.edu

Dr. T. Feng  
Department of Physics and Astronomy  
Vanderbilt University  
Nashville, TN 37235, USA

Dr. T. Feng  
Materials Science and Technology Division  
Oak Ridge National Lab  
Oak Ridge, TN 37831, USA

 The ORCID identification number(s) for the author(s) of this article can be found under <https://doi.org/10.1002/adma.201801904>.

DOI: 10.1002/adma.201801904

confinement and phonon scattering by nanostructures were the motivations. During the efforts to employ wet-chemical methodologies to synthesize thermoelectric nanomaterials in large quantities and controlled microstructures, the research communities have discovered several new effects of nanostructures that can improve the thermoelectric performance. Beyond the performance, other factors such as portability (low relative density of thermoelectric material and overall weight of the assembled module), cost, and eco-compatibility (less toxicity of the constituent elements, indicated by lower LD50 (mg kg<sup>-1</sup> rat)) were studied and optimized. Here, we would like to review the recent progress in this field. Several prospects that the unique attributes of solution-synthesized nanoparticles may revolutionize thermoelectrics are discussed in the concluding remarks.

## 2. Large-Scale Syntheses of Metal Telluride Nanomaterials for High-Performance Thermoelectrics

In the practical application of thermoelectrics, the materials should be fabricated into well-defined shapes to fit the device infrastructure. During the research and development, the evaluation of figure of merit,  $zT$ , also requires a macroscopic pellet to retrieve several physical parameters. Therefore, usually a cylinder with diameter >10 mm and thickness >10 mm should be fabricated, which weighted around 6–8 g. On the other hand, considering the material library of thermoelectrics, there are very limited categories of compounds available. In 300–500 K, Bi<sub>2</sub>Te<sub>3</sub> is the dominant compound. In 500–900 K, PbTe and CoSb<sub>3</sub><sup>[10]</sup> are the most prevalent ones. At 900–1200 K, SiGe alloy is the best choice. For the CoSb<sub>3</sub>, it is difficult to obtain Sb(0) using wet-chemical methods (usually hydride should be used as the reducing agent).<sup>[11]</sup> Similarly, the production of elemental Si<sup>[12]</sup> and Ge<sup>[13]</sup> is also challenging in solution synthesis. Therefore, the research community mainly focused on the large-scale, solution-phase syntheses of Bi<sub>2</sub>Te<sub>3</sub>, PbTe and their derivatives, such as Bi<sub>0.5</sub>Sb<sub>1.5</sub>Te<sub>3</sub> and Bi<sub>2</sub>Te<sub>2.5</sub>Se<sub>0.5</sub>, vide infra.

We would like to describe the general strategy to synthesize metal tellurides, such as Bi<sub>2</sub>Te<sub>3</sub><sup>[14]</sup> and PbTe,<sup>[15]</sup> using the method developed by Wu and co-workers as an example. In the first step, TeO<sub>2</sub>, KOH, and poly(vinylpyrrolidone) (PVP, the surfactant) were dissolved into ethylene glycol (Figure 1a,b) and heated to a designated temperature (Figure 1c). The reducing agent, hydrazine hydrate was injected to convert Te(IV) into Te(0) (Figure 1d). In the subsequent step, precursors of the metal cations (Bi(NO<sub>3</sub>)<sub>3</sub>·5H<sub>2</sub>O or Pb(CH<sub>3</sub>COO)<sub>2</sub>) were added to the dispersion of Te nanowire. The scale of this synthesis could be enlarged in a large (1000 mL) three-neck flask to yield around 10 g of product. In some instances when the nanowire was too thin, the reaction dispersion became so viscous that magnetic stirrings did not work well. Commercially available Chemglass CHEMRxnHUB reactor (Figure 1a–d) could provide a strong stirring using PTFE-coated stirring propeller and uniform heating via the jacket fluid.<sup>[16]</sup> Similarly, hydroxylamine<sup>[17]</sup> (for Bi<sub>2</sub>Te<sub>3</sub> and Bi<sub>2</sub>Se<sub>3</sub>), trioctylphosphine<sup>[18]</sup> (for Bi<sub>2</sub>Te<sub>3</sub>), and NaBH<sub>4</sub><sup>[19]</sup> (for SnSe) are commonly employed reducing agents

for the wet-chemical synthesis of nanostructured metal chalcogenides for thermoelectrics. In some instances when the cations are easily reducible (such as Ag<sup>[20]</sup> or Cu<sup>[21]</sup>), the use of aforementioned strong reducing agent can be avoided while even the solvent itself (e.g., ethylene glycol) can transform the cations and Te into metal telluride nanomaterials. Moreover, using high-temperature or high-pressure (e.g., solvothermal) reaction conditions, Bi<sub>2</sub>Te<sub>3</sub><sup>[22]</sup> or PbTe<sup>[23]</sup> nanoparticles can also be obtained using the solvent, ethylene glycol, as the reducing agent.

Based on the syntheses of metal telluride nanoparticles in large quantities (>10 g), the dried powder could be consolidated into a monolith (Figure 1e–g) using spark plasma sintering (SPS) or hot pressing. In the as-obtained pellet, detailed structural characterizations using X-ray diffraction (XRD), scanning electron microscopy (SEM) (Figure 1h–j), and transmission electron microscopy (TEM) (Figure 1n) revealed that the crystal phase was preserved and the grain size did not increase much.<sup>[14,15]</sup> The electrical conductivity and carrier mobility were impaired slightly due to the increased scattering of charge carriers cross the nanograin boundaries. Simultaneously, the thermal conductivity was also diminished due to the enhanced scattering of phonons by the nanosized grain boundaries. The numerator and the denominator of the expression of  $zT$  may compensate for each other. Resultantly, the figure of merit of solution-synthesized nanostructured pellet (Bi<sub>0.5</sub>Sb<sub>1.5</sub>Te<sub>3</sub>,  $zT = 1.96$  at 420 K;<sup>[24]</sup> Bi<sub>2</sub>Te<sub>2.7</sub>Se<sub>0.3</sub>,  $zT = 1.23$  at 488 K;<sup>[22]</sup> SnSe,  $zT = 2.1$  at 673 K;<sup>[25]</sup> or n-type PbTe,  $zT = 1.4$  at 675 K<sup>[23]</sup>) was equal to or even better than that of the solid state-processed bulk-grain or nanostructured pellet (ball-milled Bi<sub>0.5</sub>Sb<sub>1.5</sub>Te<sub>3</sub>,  $zT = 1.4$  at 373 K;<sup>[9]</sup> melt-spun Bi<sub>0.5</sub>Sb<sub>1.5</sub>Te<sub>3</sub>,  $zT = 1.86$  at 320 K;<sup>[26]</sup> ball-milled Bi<sub>2</sub>Te<sub>2.75</sub>Se<sub>0.25</sub>,  $zT = 1.18$  at 375 K;<sup>[27]</sup> single-crystal SnSe,  $zT = 2.6$  at 900 K;<sup>[28]</sup> melt-quenched polycrystalline SnSe,  $zT = 0.8$  at 800 K;<sup>[29]</sup> or melt-quenched n-type PbTe,  $zT = 1.4$  at 720 K<sup>[3]</sup>).

## 3. Fabrication of Metal Telluride Nano-Heterostructures (NHSSs) for Thermoelectrics: Synergistic Effects

Based on the synthesis of metal telluride nanomaterials using wet-chemical approaches, the researchers tried to proceed to a more sophisticated task of synthesizing nano-heterostructures. NHSSs are multicomponent nanoparticles comprised of two or more different sections that are strongly connected through chemically bonded interfaces. The motivation was to integrate the functionalities and generate synergistic properties. Basically, for different component of the nano-heterostructure, different reaction conditions should be chosen according to the reactivity of precursors.<sup>[30]</sup> For example, to synthesize PbTe–Ag<sub>2</sub>Te–PbTe NHS,<sup>[31]</sup> in the 1st step, Pb(CH<sub>3</sub>COO)<sub>2</sub> was introduced into the dispersion of as-synthesized Te nanowires containing hydrazine as the reducing agent. In the 2nd step, the dispersion was centrifuged, redispersed, and then reacted with AgNO<sub>3</sub>. Without the presence of hydrazine, ethylene glycol itself could convert Ag(I) to Ag(0). Similarly, this synthetic strategy could be utilized in the Bi<sub>2</sub>Te<sub>3</sub>–Ag<sub>2</sub>Te–Bi<sub>2</sub>Te<sub>3</sub> NHS.<sup>[32]</sup> Based on the

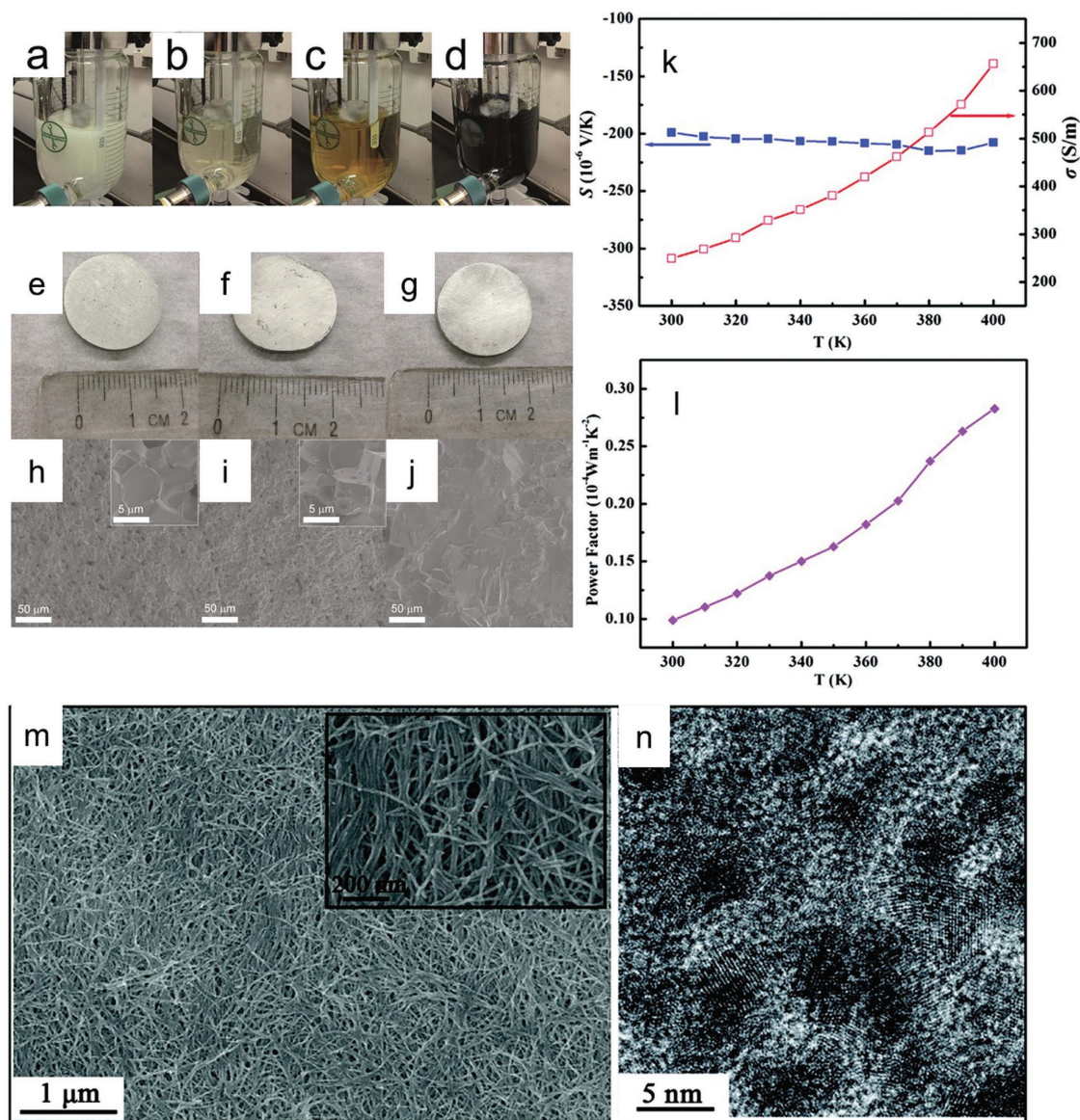


**Figure 1.** a–d) Transition of the reaction solution color at several stages of PbTe nanowire synthesis. Reproduced with permission.<sup>[16]</sup> Copyright 2014, RSC. e–g) Digital photographs of SPS 405 °C (e), SPS 450 °C (f), and SPS 500 °C (g), and h–j) SEM images of SPS 405 °C (h), SPS 450 °C (i), and SPS 500 °C (j) samples of PbTe. e–j) Reproduced with permission.<sup>[15]</sup> Copyright 2014 ACS. k) Temperature dependence of Seebeck coefficient and electrical conductivity. l) Calculated power factor for n-type Bi<sub>2</sub>Te<sub>3</sub> nanowire drop-cast films. m) Typical SEM images for Bi<sub>2</sub>Te<sub>3</sub> nanowire film, the inset is an enlarged view. n) Typical HRTEM images for Bi<sub>2</sub>Te<sub>3</sub> nanowire composites after SPS. k–n) Reproduced with permission.<sup>[14]</sup> Copyright 2012, ACS.

mentioned principle, Bi<sub>2</sub>Te<sub>3</sub>–PbTe–Bi<sub>2</sub>Te<sub>3</sub><sup>[33]</sup> NHSs could be synthesized using hydrazine as the reducing agent in both the 1st and 2nd steps because ethylene glycol itself could not transform Pb(II) and Bi(III) to their elemental states.

In the relevant studies, it was found that the NHS can introduce several advantages to boost the thermoelectric performance as compared to the single units. First, the power factor,  $S^2\sigma$ , could be enhanced using the energy filtering effect at the boundary of two semiconductor components with band edge offsets. For example, in PbTe–Ag<sub>2</sub>Te–PbTe,<sup>[31]</sup> we found that the valence band maximum (VBM) of PbTe and Ag<sub>2</sub>Te were very close to each other. Contrarily the conduction band minimum (CBM) of these two units had a much larger offset

(Figure 2e). As the total Seebeck coefficient is expressed as  $S = (S_e\sigma_e + S_h\sigma_h)/(\sigma_e + \sigma_h)$ , where n and p represent electron and hole, respectively. Based on this expression, for a p-type material, it is beneficial to enhance  $S_h$  and simultaneously suppress  $S_e$ . The different interfacial band offsets have the advantage to “filter” the holes (valence band offset: 45 meV) at a less extent than the electrons (conduction band offset: 110 meV), thus increasing the overall Seebeck coefficient (Figure 2b) as compared to pure Ag<sub>2</sub>Te. Although the  $\sigma$  of the “PbTe–Ag<sub>2</sub>Te–PbTe” sample is also deteriorated slightly due to the “filtering” effect (Figure 2a), the power factor,  $S^2\sigma$ , is enhanced by 17–38% at various temperatures (Figure 2c), when compared to the Ag<sub>2</sub>Te sample. A similar effect was also observed in a solution-processed Ag–Sb<sub>2</sub>Te<sub>3</sub>–Te



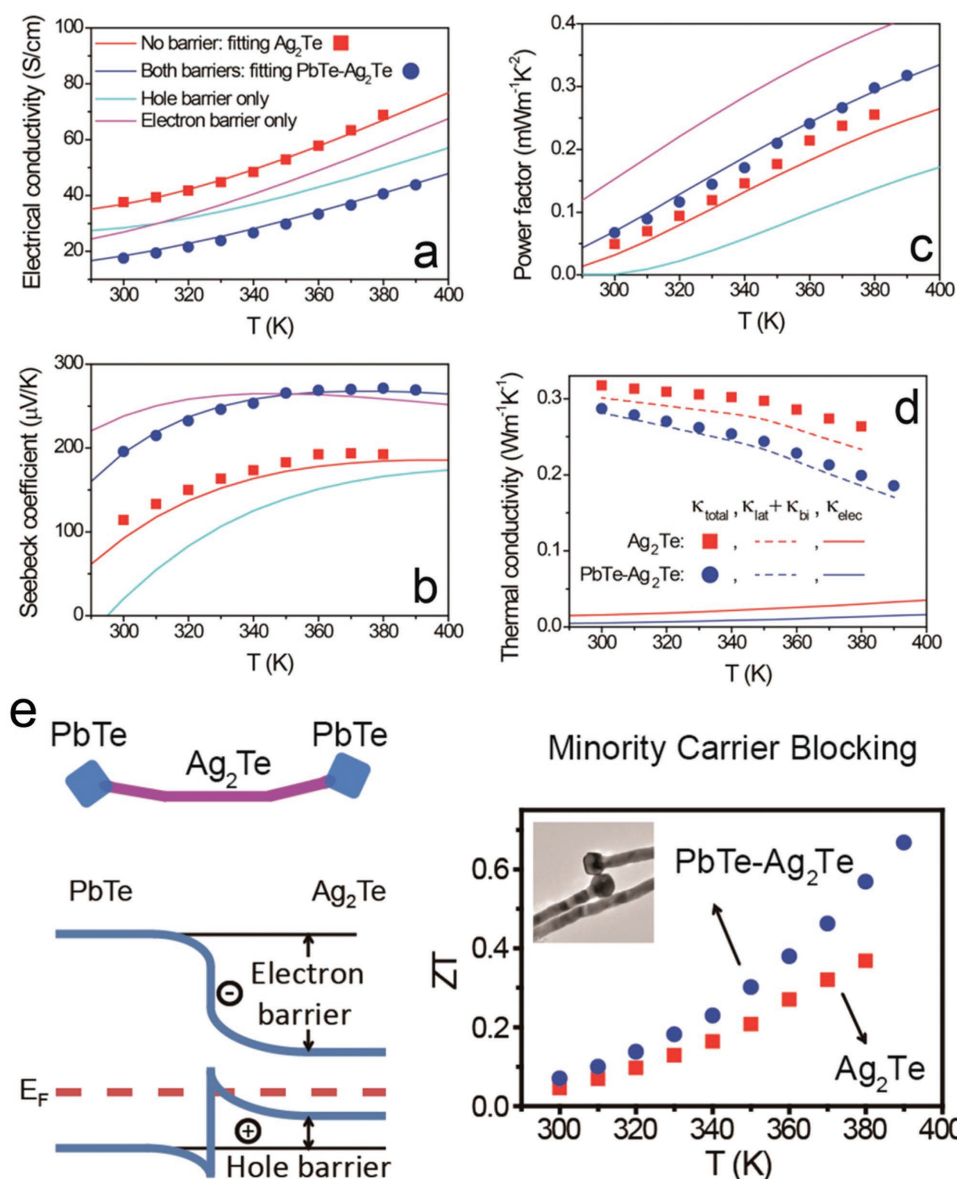


**Figure 2.** Experimental data and theoretical fitting of the thermoelectric properties. a) Electrical conductivity, b) Seebeck coefficient, c) power factor, d) thermal conductivity, and e) schematic illustration of the energy filtering effect. a–e) Reproduced with permission.<sup>[31]</sup> Copyright 2015, ACS.

heterostructure<sup>[34]</sup> and Bi<sub>2</sub>Te<sub>2</sub>·7Se<sub>0.3</sub>/Bi<sub>2</sub>Te<sub>3</sub> heterostructure.<sup>[35]</sup> This effect was also realized in a composite ball-milled Bi<sub>2</sub>Te<sub>3</sub>/solution-synthesized Bi nanomaterial.<sup>[36]</sup>

Second, the different component of the NHS may react with and diffuse into each other. In this case, the atoms in one component may serve as dopants for the other one. In the PbTe–Bi<sub>0.7</sub>Sb<sub>1.3</sub>Te<sub>3</sub> NHSs,<sup>[37]</sup> the increased carrier concentration and the steady shift of XRD peaks of the Bi<sub>0.7</sub>Sb<sub>1.3</sub>Te<sub>3</sub> matrix (Figure 3a) proved the dissolution and doping of the minor phase of PbTe into the matrix. As the doping dosage increased, the carrier concentration increased, the peak temperature of the Seebeck coefficient shifted to higher values (Figure 3b), the bandgap was enlarged due to the Burstein–Moss effect<sup>[38]</sup> (Figure 3c), and the bipolar thermal conductivity in the high-temperature range was suppressed. Collectively, the peak temperature of  $zT$  shifted to higher values

(500–650 K) as compared to that of conventional Bi<sub>x</sub>Sb<sub>2–x</sub>Te<sub>3</sub> materials (300–500 K) (Figure 3d).<sup>[9,39]</sup> A similar doping effect could also be observed in a PbTe–PtTe<sub>2</sub> NHS.<sup>[40]</sup> As the content of PtTe<sub>2</sub> increased from 0% to 30%, the original p-type ( $n = 5 \times 10^{17} \text{ cm}^{-3}$ ) PbTe turned into an n-type material ( $n = 5 \times 10^{19} \text{ cm}^{-3}$ ). Further increasing the content of PtTe<sub>2</sub> to 50% led to an increase of  $n$  to  $1 \times 10^{21} \text{ cm}^{-3}$ , indicating that Pt acted as a donor in PbTe.

Third, the nano-heterostructure contains interfaces between different components, which can enhance phonon scattering and reduce  $\kappa$ . For example, in the nanocomposite sintered from Bi<sub>2</sub>Te<sub>3</sub>–PbTe–Bi<sub>2</sub>Te<sub>3</sub> NHS, extremely low  $\kappa$  of 0.30–0.65 W m<sup>−1</sup> K<sup>−1</sup> could be attained.<sup>[33]</sup> Similarly, in the PbTe–Ag<sub>2</sub>Te–PbTe NHS, the introduction of the PbTe nano-inclusion led to diminished  $\kappa$  as compared to the single-component Ag<sub>2</sub>Te (Figure 2d).<sup>[31]</sup> This effect was first realized

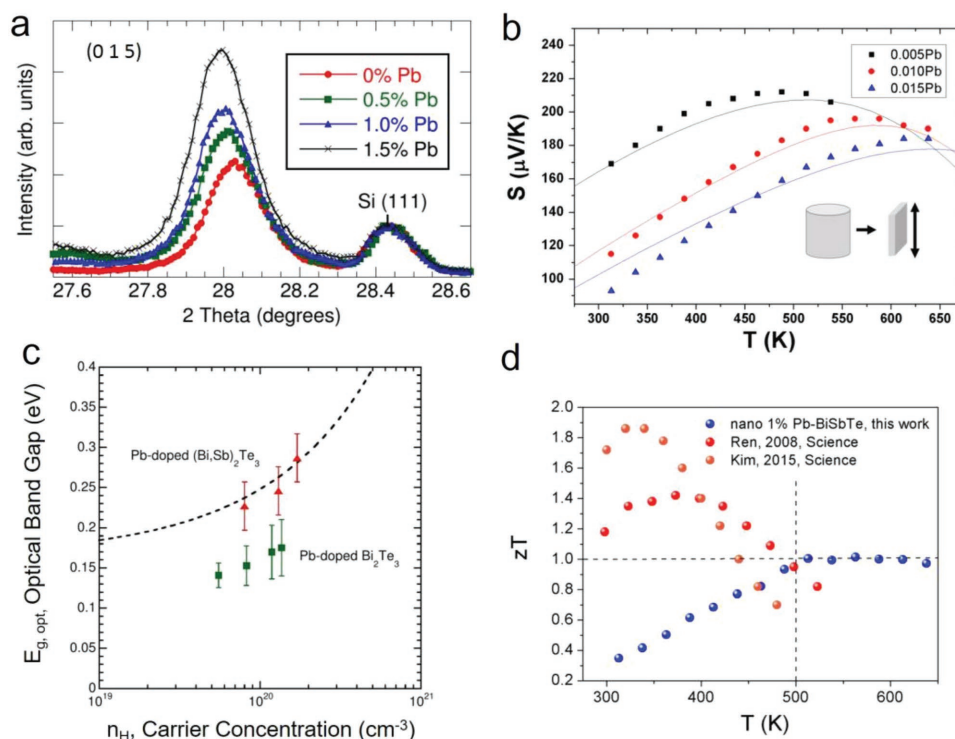


**Figure 3.** a) XRD peak shifts with nominal Pb doping; b) temperature dependence of Seebeck coefficient; c) the optical bandgap of Pb-Bi<sub>x</sub>Sb<sub>2-x</sub>Te<sub>3</sub> samples with different carrier concentrations (red triangles), as compared to single parabolic band (SPB)-derived bandgaps (dash line) and the bandgaps of Pb-doped Bi<sub>2</sub>Te<sub>3</sub> (green squares); d) the zT of 1% PbTe-Bi<sub>0.9</sub>Sb<sub>1.3</sub>Te<sub>3</sub> nanocomposite in comparison with previously reported undoped Bi<sub>x</sub>Sb<sub>2-x</sub>Te<sub>3</sub>.<sup>[9,39]</sup> a–d) Reproduced with permission.<sup>[37]</sup> Copyright 2017, Wiley-VCH.

in a solid state-processed AgPb<sub>m</sub>SbTe<sub>2+m</sub> material containing Ag-Sb-rich nanoinclusions<sup>[7]</sup> in which the nanoinclusion was formed during the melting-cooling nucleation/precipitating process. The solution process may offer better control over the size and shape of the secondary nanophase (inclusion) through tuning the precursor reactivity, concentration, and reaction temperature, etc. Similar effect can also be observed in gas-phase, sputter-coated Bi-Te core/shell hetero nanowire<sup>[41]</sup> although the scale of production is small and its thermal transport could only be measured in an MEMS device.

Through the aforementioned three mechanisms, the denominator,  $S^2\sigma T$ , could be improved and/or the numerator,  $\kappa$ , could be suppressed, collectively optimizing the zT of the NHSs. There are still rich combinations of metal telluride compounds to construct NHSs, providing rich opportunities for material explorations. Additionally, other beneficial effects, such as modulation doping<sup>[42]</sup> and resonant levels,<sup>[43]</sup> might be explored to boost the thermoelectric performance in NHS-based materials.

#### 4. Decreasing the Relative Density and Improving the Portability by Controlling the Shape of Nanocrystals

Aside from the satisfactory performance, nanostructured thermoelectric materials usually have lower relative mass

density that may arise from the irregular shape and imperfect packing of the before-sintering nanopowder, endowing them with better portability (low relative density of thermoelectric material and overall weight of the assembled module). Furthermore, the packing density and porosity of the as-sintered pellet can be deliberately tuned through controlling the internal space of the starting nanopowder. Through the aforementioned hydrazine method in Section 2, internally hollow Bi<sub>2</sub>Te<sub>2.5</sub>Se<sub>0.5</sub> nanorod could be synthesized (Figure 4c).<sup>[44]</sup> Detailed observations of the sample at each intermediate step (1st: TeSe nanorod (Figure 4a); 2nd: TeSe@Bi core/shell nanorod (Figure 4b,h); 3rd: Bi<sub>2</sub>Te<sub>2.5</sub>Se<sub>0.5</sub> hollow nanorod (Figure 4c)) indicated that the vacating process may be related to the Kirkendall effect<sup>[45]</sup> in which Te(Se) and Bi react with and diffuse into each other. Using this hollow nanoparticle as starting crystallite, one could obtain highly porous thermoelectric materials with large grain sizes (Figure 4m). Thus, the thermal conductivity was significantly reduced due to the scattering of phonons by the pores, while the electrical conductivity was still maintained a high level because of weakened scattering of electrons by the large crystal grains. An excellent zT (1.18 at 463 K) and a relative density as low as 67% could be achieved. The performance and portability were improved simultaneously. Likewise, thermoelectric PbS/PbSe hollow spheres can be synthesized through a wet-chemical method.<sup>[46]</sup> Porous SnSe<sub>1-x</sub>S<sub>x</sub> nanosheet<sup>[47]</sup> can be assembled to construct porous thermoelectric monolith with a zT of 0.12 at 310 K.

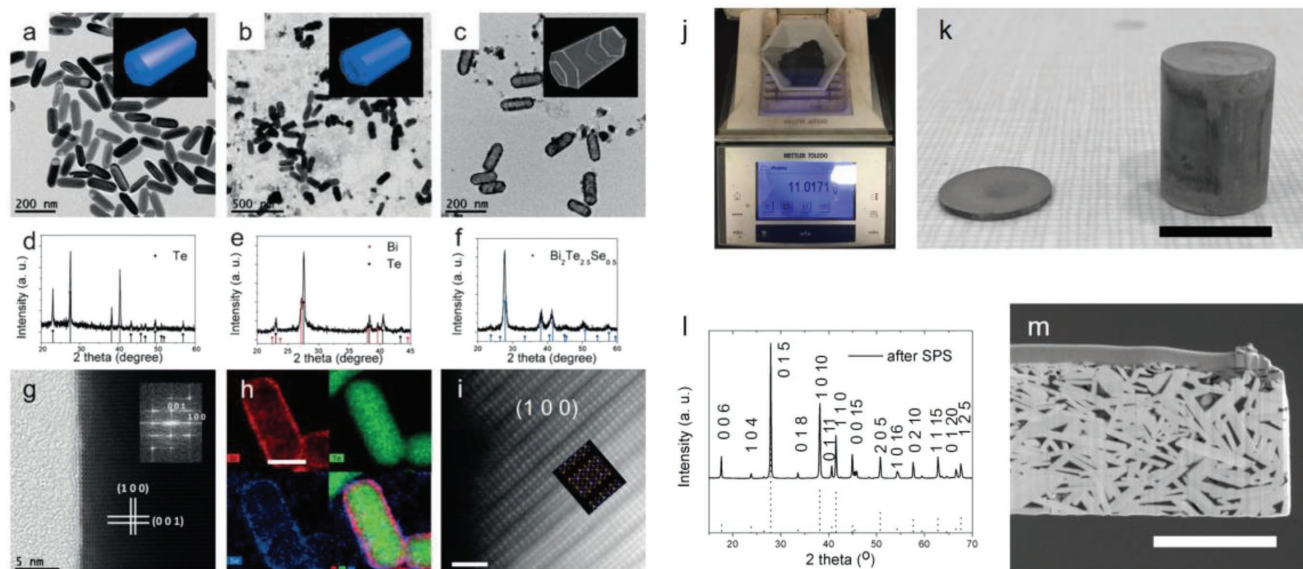


**Figure 4.** a–c) Low-magnification TEM images of: a) Te nanorods (step 1), b) Te@Bi–Se core–shell nanorods (step 2), and c)  $\text{Bi}_2\text{Te}_{2.5}\text{Se}_{0.5}$  hollow nanorods (step 3). d–f) XRD profiles of the products in each step; g) HRTEM image of the Te nanorods; h) EDS elemental mapping of the Te@Bi–Se core–shell nanorods, scale bar 50 nm; i) Cs-corrected HAADF-STEM image of the  $\text{Bi}_2\text{Te}_{2.5}\text{Se}_{0.5}$  hollow nanostructures and the corresponding atomic model of (100) surface, Bi, purple, Te(Se), orange, scale bar 1 nm; j) 11.0 g of the hollow nanostructure product; k) 400 °C sintered pellet and cylinder, scale bar 10 mm; l) XRD profile; m) SEM of the FIB-fabricated specimen, scale bar 2 mm. a–m) Reproduced with permission.<sup>[48]</sup> Copyright 2017, Wiley-VCH.

## 5. Beyond the Performance: Improving the Environmental Compatibility and Cost Efficiency

Traditional thermoelectric materials are usually comprised of expensive or toxic elements, such as Pb, Te, and Ag. To access the widespread application, these elements should be substituted by cheaper and/or nontoxic counterparts. For example, there is very low stock of tellurium (0.001 ppm) in the Earth crust, while sulfur and selenium have much higher abundance (480 and 0.05 ppm, respectively). Pb compounds (LD50: tetraethyl lead: 14 mg and lead acetate: 99 mg kg<sup>−1</sup> rat)<sup>[49]</sup> and Te (LD50 = 83 mg kg<sup>−1</sup> rat)<sup>[50]</sup> are toxic and dangerous. In contrast, Bi (Bi element, LD 50: 2000 mg kg<sup>−1</sup> rat),<sup>[51]</sup> Zn (zinc sulfate, LD 50: 623 mg kg<sup>−1</sup> rat),<sup>[52]</sup> and Sn (tin chloride, LD 50: 700–3200 mg kg<sup>−1</sup> rat)<sup>[53]</sup> are much safer with a LD50 in the order of 10<sup>3</sup> mg kg<sup>−1</sup> rat. The solution-phase syntheses of these Earth-abundant and nontoxic metal sulfide and selenide compounds as candidates for thermoelectrics have attracted extensive attentions recently.

Wu and co-workers synthesized near-stoichiometry and Cu-rich  $\text{Cu}_2\text{ZnSnS}_4$  (CZTS) nanocrystals in oleyamine.<sup>[54]</sup> For the near-stoichiometry sample, the Seebeck coefficient was as large as 450–1000  $\mu\text{V K}^{-1}$  at 300–700 K, implying its low carrier concentration. The peak  $zT$  (0.026) was comparable to that of bulk CZTS (0.039). They then intentionally increased the composition of Cu during synthesis and found that Cu(I) could act as a dopant in the  $\text{Cu}_2\text{ZnSnS}_4$  nanocrystal. The Cu-rich  $\text{Cu}_2\text{ZnSnS}_4$  nanocrystal exhibited decreased Seebeck coefficient (65–301  $\mu\text{V K}^{-1}$  at 300–700 K) and increased electrical conductivity (1388 S m<sup>−1</sup> at 700 K) as compared to the near-stoichiometry sample. More interestingly, the  $\kappa_{\text{lat}}$  of the Cu-rich sample was lower than that of the near-stoichiometry one, possibly due to the scattering of phonon by the defects at the Cu site. Consequently, the Cu-rich sample showed a much

enhanced  $zT$  (0.140 at 700 K). Similarly,  $\text{Cu}_2\text{CdSnSe}_4$ ,<sup>[55]</sup>  $\text{Cu}_2\text{ZnSnSe}_4$ ,<sup>[56]</sup> and  $\text{Cu}_2\text{ZnGeSe}_4$ <sup>[57]</sup> nanocrystals could be synthesized through solution-based routes. The solution-synthesized  $\text{Cu}_2\text{CdSnSe}_4$  ( $zT = 0.65$  at 723 K)<sup>[55]</sup> and  $\text{Cu}_2\text{ZnSnSe}_4$  ( $zT = 0.44$  at 723 K)<sup>[56]</sup> thermoelectric nanomaterial exhibited similar  $zT$  as compared to the solid-state-reacted bulk counterpart ( $\text{Cu}_2\text{CdSnSe}_4$  ( $zT = 0.65$  at 700 K)<sup>[58]</sup> and  $\text{Cu}_2\text{ZnSnSe}_4$  ( $zT = 0.50$  at 700 K)<sup>[59]</sup>).

The CZTS nanocrystal and several studies on other compounds (SnSe (nanoengineering),<sup>[19]</sup>  $\text{Cu}_5\text{FeS}_4$  (twin engineering),<sup>[60]</sup> and  $\text{Bi}_2\text{S}_3$  (nanoengineering)<sup>[61]</sup>) represented examples of structure engineering in atomic-level doping and nanolevel grain engineering of widely known compounds. Beyond this, some efforts were witnessed in synthesizing new thermoelectric metal sulfide compounds using solution-phase methods. Wu and co-workers focused on  $\text{Bi}_2\text{S}_3$ , a nontoxic and cheap metal sulfide material that still could not exceed 1.0 in  $zT$ . Iodine, another eco-friendly and cost-efficient element, was introduced during the synthesis. The I atom could serve as a template and lead to the formation of an open-framework compound,  $\text{Bi}_{13}\text{S}_{18}\text{I}_2$ .<sup>[62]</sup> Detailed analyses revealed several advantages of this compound. First, upon reconstruction of  $\text{Bi}_2\text{S}_3$  (orthorhombic), the crystal symmetry was changed to a more symmetric trigonal one ( $\text{Bi}_{13}\text{S}_{18}\text{I}_2$ ). This led to a large increment in the band degeneracy ( $N_v$ ) near the CBM from 2 ( $\text{Bi}_2\text{S}_3$ ) to 6 ( $\text{Bi}_{13}\text{S}_{18}\text{I}_2$ ). The double conduction band extrema (Figure 5a) further doubled the  $N_v$  to 12. This ultrahigh  $N_v$  could induce the extremely high Seebeck coefficient.<sup>[63]</sup> These features would lead to a high power factor since  $S^2\sigma$  was proportional to  $N_v$  at a given carrier concentration.<sup>[63]</sup>

Aside from the beneficial electronic structure, the unique atomic and phonon structure induced the extremely low  $\kappa$  of  $\text{Bi}_{13}\text{S}_{18}\text{I}_2$ . The disordered Bi(X) and I atoms had the flattest potential wells (Figure 5c) as compared with other atoms,



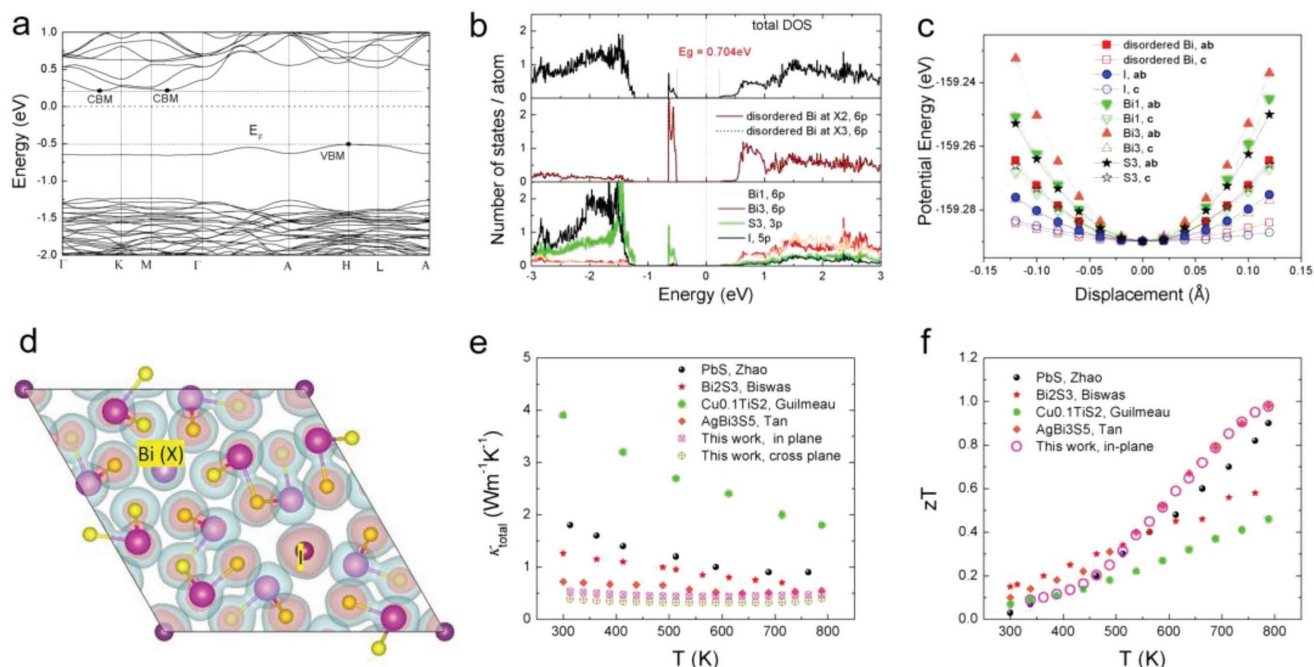


**Figure 5.** DFT calculation results: a) electronic band structure, b) density of states, c) potential wells, and d) electron localization function. Comparison of: e) total thermal conductivity,  $\kappa_{\text{total}}$ , and f) figure of merit,  $zT$ , of our “nano-Bi<sub>13</sub>S<sub>18</sub>I<sub>2</sub> + 2% BiCl<sub>3</sub>” with those of PbS,<sup>[64]</sup> Bi<sub>2</sub>S<sub>3</sub>,<sup>[65]</sup> Cu<sub>0.1</sub>TiS<sub>2</sub>,<sup>[66]</sup> and AgBi<sub>3</sub>S<sub>5</sub>.<sup>[67]</sup> Reproduced with permission.<sup>[62]</sup> Copyright 2018, Wiley-VCH.

especially along the *c*-direction. This indicated that the Bi(X) and I atoms had weakest bonding with their neighboring atoms that might lead to low-lying optical modes. These flat optical modes had very low group velocities and scatter other phonons much like so-called “rattler modes.”<sup>[68]</sup> As a result, the Bi<sub>13</sub>S<sub>18</sub>I<sub>2</sub> had  $\kappa_i$  and  $\kappa_{\text{total}}$  exceedingly low as compared to state-of-the-art n-type metal sulfide thermoelectric materials, such as Bi<sub>2</sub>S<sub>3</sub><sup>[65]</sup> and PbS<sup>[64]</sup> (Figure 5e). The peak  $zT$  of 1.0 was the highest up to date among n-type, eco-compatible and low-cost metal sulfide thermoelectric materials (Figure 5f).

Apart from the raw materials, the cost efficiency and eco-compatibility should also be considered when choosing the solvent and reducing agent. The aforementioned synthetic methods usually employed hazardous solvent or reducing agent, as exemplified by hydrazine, oleyamine, etc. Recently, Wu and co-workers succeeded in substituting the hydrazine by environment-friendly ascorbic acid.<sup>[21]</sup> In the first step, TeO<sub>2</sub> could be reduced by ascorbic acid to yield Te (0). In the following step, various metal precursors, such as bismuth nitrate, lead acetate, copper nitrate, and cadmium nitrate, could be reduced and reacted with the pre-existing Te nanowire to afford the corresponding metal telluride nanowires. Furthermore, if microwave or hydrothermal heating were employed, the solvent, ethylene glycol itself, could serve as reducing agent to produce Bi<sub>2</sub>Te<sub>2.7</sub>Se<sub>0.3</sub> nanoplates,<sup>[22]</sup> PbTe nanocubes,<sup>[23]</sup> or SnTe nanooctahedra.<sup>[69]</sup>

## 6. Conclusions and Outlook

We have reviewed the progress in solution-synthesized nanostructures for thermoelectrics. Initially, we focused on the large-scale syntheses of conventional V<sub>2</sub>VI<sub>3</sub> and IVVI thermoelectric

materials, which have achieved excellent performance. More sophisticated nano-heterostructure using elaborate multistep syntheses can introduce synergistic effects and further enhance the performance. Beyond the performance, several advantages originated from the unique microstructure of nanoparticles have been discovered to improve the portability, cost efficiency, and eco-compatibility of thermoelectric materials. We would also like to propose several prospects that nanoscience will potentially revolutionize thermoelectrics in the end.

### 6.1. Enhance the Performance by the Metastable Atomic Structures in the Nanoscale

In the nanoscale, the crystal structure of the bulk phase may be modulated due to the strongly modified thermodynamics by the large contribution from the surface energy. Hyeon and co-workers demonstrated that the perfect Te–Bi–Te–Bi–Te quintuple layer of Bi<sub>2</sub>Te<sub>3</sub> could be deviated and Bi<sub>2</sub>Te<sub>3.14</sub> with extra Te intercalated into the van der Waals gap could be formed.<sup>[70]</sup> They also claimed that this metastable structure had a modified electronic density of states that led to improved  $zT$ . Earlier studies on magic-sized metal chalcogenide nanoclusters revealed the totally disturbed atomic structure that might own distinct electronic structure.<sup>[71]</sup> These metastable nanostructures will definitely open up new avenues to optimize the thermoelectric performance.

### 6.2. Tune the Relative Density and Improve the Portability Using Shape-Controlled Nanoparticles as Building Blocks

Apart from using internally hollow nanoparticles as building blocks to construct porous thermoelectric materials,<sup>[44]</sup> the relative density can also be regulated using shape-controlled

nanoparticles with different packing perfection. For example, if branches were introduced into the nanowire, the nano-heterostructure is expected to have a lower filling fraction in the space as compared to densely packed nanowire, leading to low  $\kappa$ . If the grains simultaneously keep in large sizes and with fewer defects to suppress the scattering of electrons, a high electrical conductivity can be attained, finally leading to a high figure of merit.

### 6.3. Improving the Environmental Compatibility and Cost Efficiency of the Manufacturing Process

Apart from the raw materials, the environmental and economic concerns of the manufacturing process should also be paid attentions. Although the solution synthesis employs nontoxic precursors, solvent, and low reaction temperature, the tedious postsynthetic treatment (filtration or centrifugation) requires lot of labor and the discarded solvent containing side products is harmful. Recently, solvent-free synthesis of nanoparticles<sup>[72]</sup> has emerged and we envision that introducing this paradigm into the synthesis of thermoelectric material will probably solve the existing problems in the manufacturing.

### 6.4. Impact of Surface-Bound Ligands on the Thermoelectric Properties

How to effectively remove the organic matter on the surface of nanopowders is also a critical concern in the wet-chemical synthesis of nano-thermoelectric materials. The surfactants used in the synthesis (such as PVP and oleyamine) usually contain long chains of carbon and are considered to be electrically nonconductive. To remove these surfactants, usually ligand exchange with short-chain counterpart (such as  $N_2H_4$ ,  $SHCH_2CH_2SH$ , and  $NH_2CH_2CH_2NH_2$ )<sup>[73]</sup> or calcination<sup>[23]</sup> is a common strategy. Recently, the ligand exchange with short-chain molecules is found to significantly influence the electrical transport (carrier concentration and mobility),<sup>[73]</sup> opening a new avenue to tailor the thermoelectric properties of nanomaterials.

## Acknowledgements

B.X. thanks the support from National Natural Science Foundation of China (21801133). B.X. thanks the support from the startup funding of Nanjing University of Science and Technology (AE89991/043). B.X. and Y.W. thank the support from ACRI Center Initiative from Iowa State University and Herbert L. Stiles Professorship.

## Conflict of Interest

The authors declare no conflict of interest.

## Keywords

nanostuctures, solution, synthesis, thermoelectrics

Received: March 26, 2018

Revised: May 22, 2018

Published online: August 21, 2018

- [1] a) L. Yang, Z.-G. Chen, M. S. Dargusch, J. Zou, *Adv. Energy Mater.* **2018**, 8, 1701797; b) G. Tan, L.-D. Zhao, M. G. Kanatzidis, *Chem. Rev.* **2016**, 116, 12123.
- [2] H. J. Goldsmid, R. W. Douglas, *Br. J. Appl. Phys.* **1954**, 5, 386.
- [3] A. D. LaLonde, Y. Pei, H. Wang, G. Jeffrey Snyder, *Mater. Today* **2011**, 14, 526.
- [4] L. E. Brus, *J. Chem. Phys.* **1984**, 80, 4403.
- [5] L. D. Hicks, M. S. Dresselhaus, *Phys. Rev. B* **1993**, 47, 16631.
- [6] a) R. Venkatasubramanian, E. Siivola, T. Colpitts, B. O'Quinn, *Nature* **2001**, 413, 597; b) T. C. Harman, P. J. Taylor, M. P. Walsh, B. E. LaForge, *Science* **2002**, 297, 2229.
- [7] K. F. Hsu, S. Loo, F. Guo, W. Chen, J. S. Dyck, C. Uher, T. Hogan, E. K. Polychroniadis, M. G. Kanatzidis, *Science* **2004**, 303, 818.
- [8] a) A. I. Hochbaum, R. Chen, R. D. Delgado, W. Liang, E. C. Garnett, M. Najarian, A. Majumdar, P. Yang, *Nature* **2008**, 451, 163; b) A. I. Boukai, Y. Bunimovich, J. Tahir-Kheli, J.-K. Yu, W. A. Goddard III, J. R. Heath, *Nature* **2008**, 451, 168.
- [9] B. Poudel, Q. Hao, Y. Ma, Y. Lan, A. Minnich, B. Yu, X. Yan, D. Wang, A. Muto, D. Vashaee, X. Chen, J. Liu, M. S. Dresselhaus, G. Chen, Z. Ren, *Science* **2008**, 320, 634.
- [10] X. Shi, J. Yang, J. R. Salvador, M. Chi, J. Y. Cho, H. Wang, S. Bai, J. Yang, W. Zhang, L. Chen, *J. Am. Chem. Soc.* **2011**, 133, 7837.
- [11] a) M. He, K. Kravchyk, M. Walter, M. V. Kovalenko, *Nano Lett.* **2014**, 14, 1255; b) C. S. Birkel, E. Mugnaioli, T. Gorelik, U. Kolb, M. Panthöfer, W. Tremel, *J. Am. Chem. Soc.* **2010**, 132, 9881.
- [12] A. T. Heitsch, D. D. Fanfair, H.-Y. Tuan, B. A. Korgel, *J. Am. Chem. Soc.* **2008**, 130, 5436.
- [13] X. Lu, B. A. Korgel, K. P. Johnston, *Chem. Mater.* **2005**, 17, 6479.
- [14] G. Zhang, B. Kirk, L. A. Jauregui, H. Yang, X. Xu, Y. P. Chen, Y. Wu, *Nano Lett.* **2012**, 12, 56.
- [15] S. W. Finefrock, G. Zhang, J.-H. Bahk, H. Fang, H. Yang, A. Shakouri, Y. Wu, *Nano Lett.* **2014**, 14, 3466.
- [16] S. W. Finefrock, H. Fang, H. Yang, H. Darsono, Y. Wu, *Nanoscale* **2014**, 6, 7872.
- [17] X. Cai, W. Gao, M. Ma, M. Wu, L. Zhang, Y. Zheng, H. Chen, J. Shi, *Adv. Mater.* **2015**, 27, 6382.
- [18] a) H.-J. Kim, K.-J. Lee, S.-J. Kim, M.-K. Han, *Bull. Korean Chem. Soc.* **2010**, 31, 1123; b) J. S. Son, M. K. Choi, M.-K. Han, K. Park, J.-Y. Kim, S. J. Lim, M. Oh, Y. Kuk, C. Park, S.-J. Kim, T. Hyeon, *Nano Lett.* **2012**, 12, 640.
- [19] G. Han, S. R. Popuri, H. F. Greer, J. W. G. Bos, W. Zhou, A. R. Knox, A. Montecucco, J. Siviter, E. A. Man, M. Macauley, D. J. Paul, W. g. Li, M. C. Paul, M. Gao, T. Sweet, R. Freer, F. Azough, H. Baig, N. Sellami, T. K. Mallick, D. H. Gregory, *Angew. Chem., Int. Ed.* **2016**, 55, 6433.
- [20] H. Yang, J.-H. Bahk, T. Day, A. M. S. Mohammed, B. Min, G. J. Snyder, A. Shakouri, Y. Wu, *Nano Lett.* **2014**, 14, 5398.
- [21] H. Yang, S. W. Finefrock, J. D. Albarracin Caballero, Y. Wu, *J. Am. Chem. Soc.* **2014**, 136, 10242.
- [22] M. Hong, T. C. Chasapis, Z.-G. Chen, L. Yang, M. G. Kanatzidis, G. J. Snyder, J. Zou, *ACS Nano* **2016**, 10, 4719.
- [23] L. Yang, Z.-G. Chen, M. Hong, L. Wang, D. Kong, L. Huang, G. Han, Y. Zou, M. Dargusch, J. Zou, *Nano Energy* **2017**, 31, 105.
- [24] Y. Liu, Y. Zhang, S. Ortega, M. Ibáñez, K. H. Lim, A. Grau-Carbonell, S. Martí-Sánchez, K. M. Ng, J. Arbiol, M. V. Kovalenko, D. Cadavid, A. Cabot, *Nano Lett.* **2018**, 18, 2557.
- [25] W. Wei, C. Chang, T. Yang, J. Liu, H. Tang, J. Zhang, Y. Li, F. Xu, Z. Zhang, J.-F. Li, G. Tang, *J. Am. Chem. Soc.* **2018**, 140, 499.
- [26] S. I. Kim, K. H. Lee, H. A. Mun, H. S. Kim, S. W. Hwang, J. W. Roh, D. J. Yang, W. H. Shin, X. S. Li, Y. H. Lee, G. J. Snyder, S. W. Kim, *Science* **2015**, 348, 109.
- [27] L. Hu, H. Wu, T. Zhu, C. Fu, J. He, P. Ying, X. Zhao, *Adv. Energy Mater.* **2015**, 5, 1500411.
- [28] L.-D. Zhao, S.-H. Lo, Y. Zhang, H. Sun, G. Tan, C. Uher, C. Wolverton, V. P. Dravid, M. G. Kanatzidis, *Nature* **2014**, 508, 373.



- [29] T.-R. Wei, G. Tan, X. Zhang, C.-F. Wu, J.-F. Li, V. P. Dravid, G. J. Snyder, M. G. Kanatzidis, *J. Am. Chem. Soc.* **2016**, *138*, 8875.
- [30] L. Carbone, P. D. Cozzoli, *Nano Today* **2010**, *5*, 449.
- [31] H. Yang, J.-H. Bahk, T. Day, A. M. S. Mohammed, G. J. Snyder, A. Shakouri, Y. Wu, *Nano Lett.* **2015**, *15*, 1349.
- [32] H. Fang, H. Yang, Y. Wu, *Chem. Mater.* **2014**, *26*, 3322.
- [33] H. Fang, T. Feng, H. Yang, X. Ruan, Y. Wu, *Nano Lett.* **2013**, *13*, 2058.
- [34] Y. Zhang, J.-H. Bahk, J. Lee, C. S. Birkel, M. L. Snedaker, D. Liu, H. Zeng, M. Moskovits, A. Shakouri, G. D. Stucky, *Adv. Mater.* **2014**, *26*, 2755.
- [35] S. Li, C. Xin, X. Liu, Y. Feng, Y. Liu, J. Zheng, F. Liu, Q. Huang, Y. Qiu, J. He, J. Luo, F. Pan, *Nano Energy* **2016**, *30*, 780.
- [36] S. Sumithra, J. Takas Nathan, K. Misra Dinesh, M. Nolting Westly, P. F. P. Poudeu, L. Stokes Kevin, *Adv. Energy Mater.* **2011**, *1*, 1141.
- [37] B. Xu, M. T. Agne, T. Feng, T. C. Chasapis, X. Ruan, Y. Zhou, H. Zheng, J. H. Bahk, M. G. Kanatzidis, G. J. Snyder, *Adv. Mater.* **2017**, *29*, 1605140.
- [38] A. Walsh, J. L. F. Da Silva, S.-H. Wei, *Phys. Rev. B* **2008**, *78*, 075211.
- [39] W. Liu, H. S. Kim, S. Chen, Q. Jie, B. Lv, M. Yao, Z. Ren, C. P. Opeil, S. Wilson, C.-W. Chu, Z. Ren, *Proc. Natl. Acad. Sci. USA* **2015**, *112*, 3269.
- [40] W. Zhou, J. Zhu, D. Li, H. H. Hng, F. Y. C. Boey, J. Ma, H. Zhang, Q. Yan, *Adv. Mater.* **2009**, *21*, 3196.
- [41] J. Kang, J. W. Roh, W. Shim, J. Ham, J. S. Noh, W. Lee, *Adv. Mater.* **2011**, *23*, 3414.
- [42] D. Wu, Y. Pei, Z. Wang, H. Wu, L. Huang, L.-D. Zhao, J. He, *Adv. Funct. Mater.* **2014**, *24*, 7763.
- [43] J. P. Heremans, V. Jovovic, E. S. Toberer, A. Saramat, K. Kurosaki, A. Charoenphakdee, S. Yamanaka, G. J. Snyder, *Science* **2008**, *321*, 554.
- [44] B. Xu, T. Feng, M. T. Agne, L. Zhou, X. Ruan, G. J. Snyder, Y. Wu, *Angew. Chem., Int. Ed.* **2017**, *56*, 3546.
- [45] Y. Yin, R. M. Rioux, C. K. Erdonmez, S. Hughes, G. A. Somorjai, A. P. Alivisatos, *Science* **2004**, *304*, 711.
- [46] R. Jin, G. Chen, J. Pei, *J. Phys. Chem. C* **2012**, *116*, 16207.
- [47] H. Ju, M. Kim, D. Park, J. Kim, *Chem. Mater.* **2017**, *29*, 3228.
- [48] C. C. Dun, C. A. Hewitt, Q. Li, Y. Guo, Q. K. Jiang, J. W. Xu, G. Marcus, D. C. Schall, D. L. Carroll, *Adv. Mater.* **2017**, *29*, 1702968.
- [49] a) J. Schubert, E. J. Riley, S. A. Tyler, *J. Toxicol. Environ. Health* **1978**, *4*, 763; b) T. Schroeder, D. D. Avery, H. A. Cross, *Experientia* **1972**, *28*, 425.
- [50] R. Agrawal Meena, C. Winder, *J. Appl. Toxicol.* **1996**, *16*, 407.
- [51] Y. Sano, H. Satoh, M. Chiba, M. Okamoto, K. Serizawa, H. Nakashima, K. Omae, *J. Occup. Health* **2005**, *47*, 293.
- [52] J. Domingo, J. Llobet, J. Paternain, J. Corbella, *Vet. Hum. Toxicol.* **1988**, *30*, 224.
- [53] S. Blunden, T. Wallace, *Food Chem. Toxicol.* **2003**, *41*, 1651.
- [54] H. Yang, L. A. Jauregui, G. Zhang, Y. P. Chen, Y. Wu, *Nano Lett.* **2012**, *12*, 540.
- [55] F.-J. Fan, B. Yu, Y.-X. Wang, Y.-L. Zhu, X.-J. Liu, S.-H. Yu, Z. Ren, *J. Am. Chem. Soc.* **2011**, *133*, 15910.
- [56] F. J. Fan, Y. X. Wang, X. J. Liu, L. Wu, S. H. Yu, *Adv. Mater.* **2012**, *24*, 6158.
- [57] M. Ibáñez, R. Zamani, A. LaLonde, D. Cadavid, W. Li, A. Shavel, J. Arbiol, J. R. Morante, S. Gorsse, G. J. Snyder, A. Cabot, *J. Am. Chem. Soc.* **2012**, *134*, 4060.
- [58] M. L. Liu, I. W. Chen, F. Q. Huang, L. D. Chen, *Adv. Mater.* **2009**, *21*, 3808.
- [59] M.-L. Liu, F.-Q. Huang, L.-D. Chen, I. W. Chen, *Appl. Phys. Lett.* **2009**, *94*, 202103.
- [60] A. Zhang, B. Zhang, W. Lu, D. Xie, H. Ou, X. Han, J. Dai, X. Lu, G. Han, G. Wang, X. Zhou, *Adv. Funct. Mater.* **2018**, *28*, 1705117.
- [61] W. Liu, C. F. Guo, M. Yao, Y. Lan, H. Zhang, Q. Zhang, S. Chen, C. P. Opeil, Z. Ren, *Nano Energy* **2014**, *4*, 113.
- [62] B. Xu, T. Feng, M. T. Agne, Q. Tan, Z. Li, K. Imasato, L. Zhou, J. H. Bahk, X. Ruan, G. J. Snyder, Y. Wu, *Angew. Chem., Int. Ed.* **2018**, *57*, 2413.
- [63] Y. Pei, A. D. LaLonde, H. Wang, G. J. Snyder, *Energy Environ. Sci.* **2012**, *5*, 7963.
- [64] L.-D. Zhao, S.-H. Lo, J. He, H. Li, K. Biswas, J. Androulakis, C.-I. Wu, T. P. Hogan, D.-Y. Chung, V. P. Dravid, M. G. Kanatzidis, *J. Am. Chem. Soc.* **2011**, *133*, 20476.
- [65] K. Biswas, L.-D. Zhao, M. G. Kanatzidis, *Adv. Energy Mater.* **2012**, *2*, 634.
- [66] E. Guilmeau, Y. Bréard, A. Maignan, *Appl. Phys. Lett.* **2011**, *99*, 052107.
- [67] G. Tan, S. Hao, J. Zhao, C. Wolverton, M. G. Kanatzidis, *J. Am. Chem. Soc.* **2017**, *139*, 6467.
- [68] M. Christensen, A. B. Abrahamsen, N. B. Christensen, F. Juranyi, N. H. Andersen, K. Lefmann, J. Andreasson, C. R. H. Bahl, B. B. Iversen, *Nat. Mater.* **2008**, *7*, 811.
- [69] Z. Li, Y. Chen, J.-F. Li, H. Chen, L. Wang, S. Zheng, G. Lu, *Nano Energy* **2016**, *28*, 78.
- [70] K. Park, K. Ahn, J. Cha, S. Lee, S. I. Chae, S.-P. Cho, S. Ryee, J. Im, J. Lee, S.-D. Park, M. J. Han, I. Chung, T. Hyeon, *J. Am. Chem. Soc.* **2016**, *138*, 14458.
- [71] T. Vossmeier, G. Reck, L. Katsikas, E. T. K. Haupt, B. Schulz, H. Weller, *Science* **1995**, *267*, 1476.
- [72] L. Zhang, G. Xie, J. Hui, B. Xu, G. Xiang, X. Wang, *RSC Adv.* **2012**, *2*, 3204.
- [73] Y. Sun, H. Fang, L. Pan, M. Han, S. Xu, X. Wang, B. Xu, Y. Wu, *Nano Lett.* **2015**, *15*, 3748.